A Theory for the Statistical Equilibrium Energy Spectrum and Heat Flux Produced by Transient Baroclinic Waves

BRIAN F. FARRELL

Department of Earth and Planetary Sciences, Harvard University, Cambridge, Massachusetts

PETROS J. IOANNOU

Center for Meteorology and Physical Oceanography, Massachusetts Institute of Technology, Cambridge, Massachusetts

(Manuscript received 10 May 1993, in final form 4 November 1993)

ABSTRACT

Obtaining a physically based understanding of the variations with spatial scale of the amplitude and dispersive properties of midlatitude transient baroclinic waves and the heat flux associated with these waves is a central goal of dynamic meteorology and climate studies. Recently, stochastic forcing of highly nonnormal dynamical systems, such as arise from analysis of the equations governing perturbations to the midlatitude westerly jet, has been shown to induce large transfers of energy from the mean to the perturbation scale. In the case of a baroclinic atmospheric jet, this energy transfer to the synoptic scale produces dispersive properties, distributions of wave energy with wavenumber, and heat fluxes that are intrinsically associated with the nonnormal dynamics underlying baroclinic wave development.

In this work a method for calculating the spectrum and heat flux arising from stochastic forcing is described and predictions of this theory for a model atmosphere are compared with observations. The calculated energy spectrum is found to be in remarkable agreement with observations, in contrast with the predictions of modal instability theory. The calculated heat flux exhibits a realistic distribution with height and its associated energetic cycle agrees with observed seasonal mean energetics.

1. Introduction

The large-scale dynamics of the midlatitude atmosphere is dominated by baroclinic waves drawing their energy from the mean potential energy of the jet, which is in approximate thermal wind balance with the meridional temperature gradient. In addition to their role in organizing the local wind and precipitation fields on synoptic scales, these waves are also responsible for much of the meridional transport of heat and momentum in the midlatitude troposphere. Because of their importance to both weather and climate, gaining a physical understanding of the origin, maintenance, and statistical properties of baroclinic waves has been a central theme in dynamic meteorology, and this interest has resulted in a variety of proposed explanations and theoretical constructs. These ideas include the view that latent heat release alone gives rise to cyclones (Ferrel 1881) and the conjecture that the midlatitude jet is spontaneously unstable to exponentially growing modal waves (Solberg 1928; Charney 1947; Eady 1949). Recently, it was shown that perturbation growth such as is associated with cyclogenesis can arise from transient development of nonmodal perturbations (Farrell 1982, 1984, 1985, 1989). Although this transient growth mechanism involves the same baroclinic energy source as gives rise to the more familiar exponentially unstable baroclinic waves, the flow need not support exponential instabilities for transient baroclinic wave development to occur; so it follows, for instance, that integral theorems for the existence of exponential instabilities need not be restrictive of disturbance growth in flows dominated by transient growth (cf. Charney and Stern 1962).

Regardless of whether the time mean baroclinic state of the atmosphere supports an unstable mode, observations reveal that the time and space scales over which disturbances are correlated [$\approx O(6)$ days (Leith 1973)] are insufficient for modal dominance to arise from exponential growth of initial perturbations not initiated with normal-mode form given that a subset of perturbations can be shown to grow far more rapidly [Farrell (1989) and Lin and Pierrehumbert (1988) argue that a realistic modal e-folding is $O(3)$ days at the largest synoptic scales and over the oceans].

In this work we assume that the atmosphere can be modeled as asymptotically stable (all eigenvalues correspond to asymptotic decay). We believe that observed resemblance between the normal-mode struc-

Corresponding author address: Dr. Brian F. Farrell, Department of Earth and Planetary Sciences, Harvard University, Pierce Hall, 29 Oxford St., Cambridge, MA 02138.

ture and dispersive properties and the structure and dispersive properties of baroclinic waves arises because the normal modes are structurally similar to preferred response structures under unbiased forcing. In the stochastic analysis presented in Farrell and Ioannou (1993b) this property of the modes was expressed in the analysis by the fact that the modes gave rise to poles in the expansion of the resolvent. However, while a normal dynamical system's response can be identified with the modes associated with singularities in the resolvent, we will see that this identification is considerably obscured as the nonnormality of the system increases so that a distorted picture of the mode emerges in the response of the nonnormal system.

A comprehensive theory of baroclinic dynamics should permit calculation of the statistical average spectral distribution of the dominant synoptic-scale waves as well as of the heat flux resulting from these waves. A problem of long standing in the dynamics of the midlatitude atmosphere is that of reconciling the observed dominance of global wavenumbers near 5 in the transient energy spectrum with the inviscid exponential modal instability of linearized GCMs at global wavenumber 12–15 (Gall et al. 1979). The resolution of this difficulty has been traditionally ascribed to the intercession of some nonlinear equilibration phenomenon, as was originally suggested by Gall (1976). As we will show, however, failure to obtain the observed spectra is not a fault of linear theory itself but rather of its application. When the subcritical linear operator is forced stochastically, the underlying structure of its response is revealed to be that of the observations.

While observations show the heat flux on the largest space and time scale to be adequately modeled over the seasonal cycle by an approximately linear flux/gradient relationship (Sellers 1969; North 1975; Oort and Peixoto 1983), predictions based on baroclinic theory vary widely. Using the concept of baroclinic adjustment, Stone (1978), Lindzen and Farrell (1980), and Lindzen (1993) predict that the gradient is relaxed to marginal stability by the waves, which produce whatever flux is necessary to accomplish this stabilization. Using arguments based on mixing length theory and the structure of exponential unstable waves, Green (1970) predicted a quadratic relationship between the meridional temperature gradient and the heat flux, while Held (1978) using similar methods obtained powers of 2 and 5, depending on the relative dominance of the β effect. While diffusion appears to be adequate for the purpose of constructing simple climate models and the coefficient of diffusion required by such a model can be determined empirically, from the point of view of dynamics a more fundamental understanding is desirable. One might hope that such a deeper understanding would lead to a more accurate parameterization, but regardless of whether a simple parameterization arises from this study, understanding the underlying physics remains an important goal.

The central idea of this work is that the dynamics of baroclinic waves in strong shear is dominated by differential advection, which is reflected in the nonnormality of the linear operator and that the role of nonlinearities, while important, can be parameterized. The analytic technique used to determine the baroclinic wave spectrum and heat flux makes use of recent results in the stochastic dynamics of nonnormal systems (Farrell and Ioannou 1993a,b,c).

2. Formulation

a. The model

Consider a baroclinic shear flow strongly maintained by thermal forcing, as is the case in the earth's midlatitude jets. We wish to determine the statistical equilibrium variance and heat flux resulting from stochastic excitation of this background state. The variance and quadratic perturbation fluxes are assumed to be adequately modeled by quasigeostrophic linear dynamics, which forms the basis of the theory. The effects of nonlinearity are parameterized in the theory by choosing an appropriate stochastic forcing amplitude and dissipation. Interior radiative dissipation and wave–wave-induced decorrelation are modeled by constant linear damping, while surface-induced spindown is modeled by Ekman damping. We assume a pure baroclinic flow confined to a channel bounded by rigid walls in the meridional direction y to the interval $-y_c \leq y \leq y_c$ and in the vertical direction z between the ground and a lid that will be taken to be located at $z_t = 50$ km. The effects of sphericity are represented by the β-plane approximation; that is, the Coriolis parameter is taken as $f = f_0 + \beta y$. Vertical density variation with a constant scale height

$$H = -\frac{1}{\rho}\frac{d\rho}{dz}$$

is allowed, and vertical variation of the Brunt-Väisälä frequency N is included to model the troposphere–stratosphere stability transition.

With these assumptions the quasigeostrophic perturbation potential vorticity equation can be separated and the continuous system reduced through discretization in the vertical to a finite dimensional system. The evolution of a single harmonic disturbance $u_i(t)e^{ikx}\cos(ly)$, with k and l the zonal and meridional wavenumbers, respectively, can be put in the form (Farrell and Ioannou 1993b)

$$\frac{du_i}{dt} = \mathscr{A}_{ij}u_j + \mathscr{F}_{ij}\xi_j, \tag{2.1}$$

where u_i is the generalized velocity at the ith grid. The generalized velocity u_i is defined so that the perturbation energy per unit area is given by $E = u_i^* u_i$ (we denote complex conjugation by an asterisk, and here and in the sequel the summation convention will be

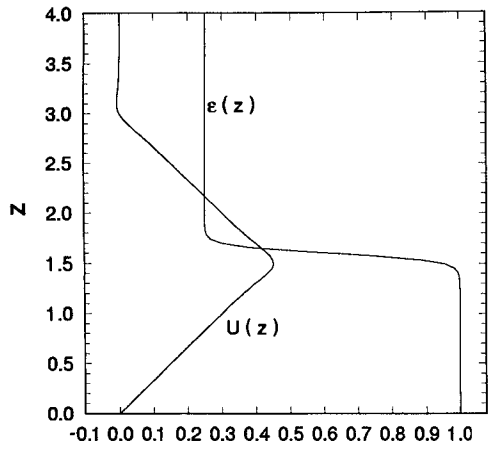

FIG. 1. The nondimensional mean flow velocity and Brunt–Väisälä frequency variation with height. The nondimensional shear $s = 0.3$ corresponds to a dimensional maximum zonal velocity of 35 m s^{-1}, and ϵ in the troposphere corresponds to Brunt–Väisälä frequency $N = 10^{-2}$ s^{-1}. The tropopause is located at nondimensional height $z = 1.5$.

used). The random forcing is taken to be a δ-correlated Gaussian white noise process with zero mean,

$$\langle \xi_i \rangle = 0, \tag{2.2a}$$

and with second moments,

$$\langle \xi_i^*(t)\xi_j(s)\rangle = \sigma^2\delta_{ij}\delta(t-s), \tag{2.2b}$$

where we denote the ensemble average operation by angle brackets. Such a random forcing excites independently and with equal magnitude σ each of the vertical forcing distributions specified by the columns of the matrix $\mathscr{F}$.

In nondimensional variables, the dynamical operator $\mathscr{A}$ is given by

$$\mathscr{A} = \mathscr{M}^{1/2}\mathscr{B}\mathscr{M}^{-1/2}, \tag{2.3}$$

where

$$\mathscr{M} = \frac{h}{2}[(\mathscr{E}\mathscr{T})^\dagger\mathscr{E}\mathscr{T} + \alpha^2\mathscr{P}^2], \tag{2.4}$$

and $\mathscr{B}$ is the discretized differential operator,

$$\mathscr{B} = \frac{e^{z/2}}{\sqrt{\epsilon}}(\Delta^{-1}(-ikU - R)\Delta - ik\Delta^{-1}Q_y)\frac{\sqrt{\epsilon}}{e^{z/2}}, \tag{2.5}$$

where

$$\Delta = \frac{\partial^2}{\partial z^2} - \left(\frac{\alpha^2}{\epsilon} + S^2 - \frac{dS}{dz}\right), \tag{2.6}$$

and where the operator Δ^{-1} has been rendered unique through incorporation of the boundary conditions. In the above relations, h is the grid interval, $\alpha = \sqrt{k^2 + l^2}$ is the total horizontal wavenumber, $\mathscr{T}$ is the discretized first-order d/dz operator, $\mathscr{P}_{ij} = \sqrt{\rho^{(i)}}\delta_{ij}$, and $\mathscr{E}_{ij} = \sqrt{\rho^{(i)}\epsilon^{(i)}}\delta_{ij}$, with ϵ being the stratification parameter defined below and with the superscript (i) denoting the value of a variable at the ith grid point.

The nondimensional zonal wind assumed to have the form

$$U = sz - [sz - s(z - z_0)]\frac{1 + \tanh[(z - z_0)/\delta]}{2} + s(z - z_0)\frac{1 + \tanh[(z - 2z_0)/\delta]}{2}, \tag{2.7}$$

with the nondimensional shear parameter denoted by s. The jet maximum occurs $z_0 = 1.5$ and has a depth scale $\delta = 0.15$.

The nondimensional stratification parameter assumed to have the form

$$\epsilon = \left[1 + 3\frac{1 + \tanh[(z - z_s)/\delta_s]}{2}\right]^{-1} \tag{2.8}$$

with $z_s = z_0 + \delta$ and $\delta_s = \delta/2$. The mean potential vorticity gradient is given by

$$Q_y = \frac{\beta}{\epsilon} + 2S\frac{dU}{dz} - \frac{d^2U}{dz^2}, \tag{2.9}$$

and the stability parameter by

$$S = -\frac{1}{2}\left(\frac{1}{\epsilon}\frac{d\epsilon}{dz} - 1\right). \tag{2.10}$$

A typical vertical distribution of the mean flow and the stratification parameter ϵ is shown in Fig. 1. In Fig. 2 we plot the vertical distribution of the mean potential vorticity gradient.

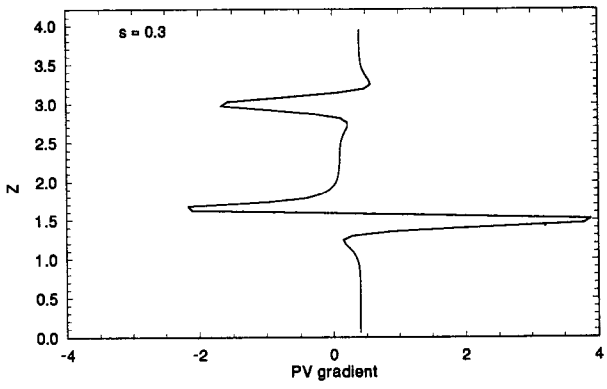

FIG. 2. The nondimensional mean flow potential vorticity gradient in the interior of the flow as a function of height. The parameters are the same as those in Fig. 1. The equivalent δ function contribution at the surface arising from the surface temperature gradient is not shown.

In (2.5) R represents a constant linear damping in addition to which surface boundary-layer dissipation is included with Ekman damping parameter

$$\Gamma_0 = \frac{i}{H}\left(\frac{\nu}{2f_0}\right)^{1/2}\frac{\alpha^2}{\epsilon k}, \tag{2.11}$$

where ν is the coefficient of vertical eddy diffusion.

In these equations time has been nondimensionalized by $1/f_0$, vertical distance by H, and horizontal distance by $L = H/\sqrt{\epsilon_0}$, where $\epsilon_0 = f_0^2/N_0^2$ is the square of the ratio of the Coriolis parameter f_0 to a characteristic Brunt–Väisälä frequency N_0. The dimensional variables (denoted with a tilde) are

$$\begin{aligned}
\tilde{t} &= \frac{t}{f_0}\\
\tilde{k} &= \frac{\sqrt{\epsilon_0}k}{H}\\
\tilde{l} &= \frac{\sqrt{\epsilon_0}l}{H}\\
\tilde{z} &= Hz\\
\tilde{U} &= f_0 L U\\
\tilde{\epsilon} &= \epsilon_0\epsilon\\
\tilde{\beta} &= \frac{f_0\sqrt{\epsilon_0}\beta}{H}.
\end{aligned} \tag{2.12}$$

The dimensional generalized velocity is

$$\tilde{u}_i = \sqrt{\rho_g} f_0 L\sqrt{H} u_i, \tag{2.13}$$

and the random forcing is

$$\tilde{\xi}_i = \sqrt{\rho_g} f_0^2 L\sqrt{H}\xi_i, \tag{2.14}$$

where ρ_g is the density at the ground.

Values of parameters appropriate for the midlatitude atmosphere at 45°N were chosen: $f_0 = 10^{-4}\ \mathrm{s}^{-1}$, $N = 10^{-2}\ \mathrm{s}^{-1}$, $H = 7.5$ km, $L = 750$ km, and $\tilde{\beta} = 1.6 \times 10^{-11}\ \mathrm{m}^{-1}\ \mathrm{s}^{-1}$. These parameter values result in $\beta = 0.12$, a wave with zonal wavelength of 4700 km corresponding to horizontal wavenumber $k = 1$, and a unit of nondimensional time corresponding to 2.8 h. Unless otherwise stated, $\nu = 20\ \mathrm{m}^2\ \mathrm{s}^{-1}$ corresponding to a square root vertical Ekman number

$$E_V^{1/2} = \frac{1}{H}\left(\frac{\nu}{2f_0}\right)^{1/2} = 0.042.$$

b. Determining the ensemble average energy

We obtain from (2.1) the ensemble energy equation

$$\frac{dE'}{dt} = \langle u_i^*(\mathcal{A}_{ij} + \mathcal{A}_{ij}^\dagger)u_j\rangle + \langle u_i^*\mathcal{F}_{ij}\xi_j + u_i\mathcal{F}_{ij}^*\xi_j^*\rangle, \tag{2.15}$$

where $E' = \langle u_i^* u_i\rangle$ is the ensemble average energy per unit area and the dagger denotes the Hermitian transpose. Considering only the inhomogeneous solution to (2.1), we can write

$$u_i = \int_0^t e_{ia}^{A(t-s)}\mathcal{F}_{ab}\xi_b(s)ds, \tag{2.16}$$

and evaluate the energy input making use of the following result:

$$\begin{aligned}
\langle u_i^*\mathcal{F}_{ij}\xi_j\rangle &= \int_0^t e_{ia}^{\mathcal{A}^*(t-s)}\mathcal{F}_{ab}^*\mathcal{F}_{ij}\langle\xi_b^*(s)\xi_j(t)\rangle ds\\
&= \sigma^2\int_0^t e_{ia}^{\mathcal{A}^*(t-s)}\mathcal{F}_{ab}^*\mathcal{F}_{ij}\delta_{bj}\delta(t-s)ds\\
&= \frac{\sigma^2}{2}\,\mathrm{trace}\,(\mathcal{F}\mathcal{F}^\dagger).
\end{aligned} \tag{2.17}$$

Use of (2.17) reduces the energy equation to

$$\frac{dE'}{dt} = \langle u_i^*(\mathcal{A}_{ij} + \mathcal{A}_{ij}^\dagger)u_j\rangle + \dot{\xi}\,\mathrm{trace}(\mathcal{F}\mathcal{F}^\dagger). \tag{2.18}$$

We consider orthonormal forcing distributions that need not be of full rank but that in any case satisfy

$$\mathrm{trace}\,(\mathcal{F}\mathcal{F}^\dagger) = N_f,$$

where N_f is the number of degrees of freedom that are forced. Hence the total rate of energy input per unit area (W m^{-2}) is $\dot{E}_{in} = \rho_g f_0^3 L^2 H N_f \sigma^2$, giving

$$\sigma^2 = \frac{\dot{E}_{in}}{N_f\rho_g f_0^3 L^2 H}. \tag{2.19}$$

Using (2.16), the nondimensional ensemble average energy per unit area can be expressed in terms of the correlation matrix $\mathcal{C}^t$:

$$\begin{aligned}
E' &= \langle u_i^* u_i\rangle\\
&= \sigma^2\,\mathrm{trace}\left(\int_0^t e^{\mathcal{A}(t-s)}\mathcal{F}\mathcal{F}^\dagger e^{\mathcal{A}^\dagger(t-s)}ds\right)\\
&= \sigma^2\,\mathrm{trace}(\mathcal{C}^t).
\end{aligned} \tag{2.20}$$

It can be shown (cf. Farrell and Ioannou 1993b) that the correlation matrix satisfies the dynamical equation

$$\frac{d\mathcal{C}^t}{dt} = \mathcal{F}\mathcal{F}^\dagger + \mathcal{A}\mathcal{C}^t + \mathcal{C}^t\mathcal{A}^\dagger, \tag{2.21}$$

with initial condition $\mathcal{C}^0 = 0$. Note also that when the orthonormal forcing distributions are of full rank in the space spanned by their range, the correlation matrix is independent of the particular forcing specification (Farrell and Ioannou 1993c).

The ensemble average energy is given in dimensional variables by

$$\tilde{E}^t = \rho_g f_0^2 L^2 H\sigma^2\,\mathrm{trace}(\mathcal{C}^t). \tag{2.22}$$

Combining (2.22) and (2.19), the dimensional energy per unit area (units: J m^{-2}) in terms of the total rate of energy input per unit area is

$$\widetilde{E}^t = \frac{\dot{E}_{in}}{f_0} \frac{\text{trace}(\mathscr{C}^t)}{N_f}. \tag{2.23}$$

c. Determining the ensemble average energetics

We write the energy transfer rate between the mean and eddies in the form (Pedlosky 1990)

$$\widetilde{T}^t = \frac{\rho_g f_0^3 L^4 \epsilon_0}{H} \left\langle \int_0^{z_t} \rho \epsilon \frac{dU}{dz} \overline{\frac{\partial \phi}{\partial x} \frac{\partial \phi}{\partial z}} dz \right\rangle, \tag{2.24}$$

where the overbar denotes an average over a zonal wavelength λ:

$$\overline{\frac{\partial \phi}{\partial x} \frac{\partial \phi}{\partial z}} = \frac{1}{\lambda} \int_0^{\lambda} \frac{\partial \phi}{\partial x} \frac{\partial \phi}{\partial z} dx = \frac{k}{2} \text{Im}\left(\phi^* \frac{\partial \phi}{\partial z} \right). \tag{2.25}$$

The energy transfer relation can be expressed in terms of our discrete correlation quantities as

$$\begin{aligned} \widetilde{T}^t &= \frac{\rho_g f_0^3 L^4 \epsilon_0}{H} h\sigma^2 \,\text{trace}(\mathscr{D}\mathscr{H}^t) \\ &= \dot{E}_{in} \frac{h \,\text{trace}(\mathscr{D}\mathscr{H}^t)}{N_f}. \end{aligned} \tag{2.26}$$

The variable ϕ is the streamfunction, which is related to the generalized velocity by $u = \mathscr{M}^{1/2}\phi$; $\mathscr{D}_{ij} = \epsilon^{(i)}(dU^{(i)}/dz)\delta_{ij}$, and

$$\mathscr{H}^t = \frac{k}{2} \text{Im}(\mathscr{P}\mathscr{T}\mathscr{M}^{-1/2}\mathscr{C}^t\mathscr{M}^{-1/2}\mathscr{P}), \tag{2.27}$$

where $\mathscr{C}^t$ is the correlation matrix determined by (2.21), $\mathscr{T}$ is the discretized d/dz operator, and $\mathscr{P}_{ij} = \sqrt{\rho^{(i)}}\delta_{ij}$. Note that the only term in (2.27) that can have an imaginary component is $\mathscr{C}^t$. The heat flux and the conversion terms consequently arise from nonnormality of the operator $\mathscr{A}$ (when $\mathscr{A}$ is normal $\mathscr{C}^t$ is real).

In dimensional variables the dissipation rate due to linear damping is

$$D_{\text{atm}} = \dot{E}_{in} R \frac{\text{trace}(\mathscr{C}^t)}{N_f}. \tag{2.28}$$

The dissipation rate at the ground due to Ekman pumping, D_{Ekman}, can be most easily calculated as a residual from the energy equation (2.18) by assuming that a statistically steady state has been reached and that the total energy is stationary.

d. Determining the ensemble average heat flux

The ensemble average heat flux (units: W m^{-1}) is defined as

$$H^t = c_p \left\langle \int_0^{z_t} \rho \overline{v\theta} dz \right\rangle, \tag{2.29}$$

where c_p is the specific heat at constant pressure;

$$v = f_0 L \frac{\partial \phi}{\partial x} \tag{2.30}$$

is the northward eddy velocity; the eddy potential temperature is

$$\theta = \frac{\Theta_g f_0^2 L^2}{gH} \frac{\partial \phi}{\partial z}, \tag{2.31}$$

where Θ_g is the potential temperature at the ground; and g is the gravitational acceleration. The ensemble average heat flux can then be written (cf. Farrell and Ioannou 1993b):

$$\begin{aligned} H^t &= \frac{c_p \rho_g \Theta_g f_0^3 L^3}{g} \left\langle \int_0^{\infty} \rho \overline{\frac{\partial \phi}{\partial x} \frac{\partial \phi}{\partial z}} dz \right\rangle \\ &= \frac{c_p \Theta_g L}{gH} \dot{E}_{in} \frac{h \,\text{trace}(\mathscr{H}^t)}{N_f}. \end{aligned} \tag{2.32}$$

In the formulation up to this point no assumption has been necessary concerning the existence of a statistically steady state as $t \to \infty$. When the dynamical operator $\mathscr{A}$ is asymptotically stable, that is, all its eigenvalues have negative real parts, then such a state is reached and $t \to \infty$ asymptotic values of the ensemble average energy and heat flux can be readily evaluated. In the following, we will consider asymptotically stable flows, stabilized by allowing the linear potential vorticity damping, R, to assume values for which the stability of the flow is ensured.

3. Results

We assume random forcing concentrated in the troposphere with a minimum vertical scale of 100 m. This limitation on the vertical scale of the forcing restricts the forcing to the first 30 Fourier harmonics in the troposphere ($0 \leq z \leq 1.5$). Note from the definition of the generalized velocity forcing in (2.1) that it includes both momentum and thermal forcing. The effect of either thermal or momentum forcing in isolation was not investigated because it can be shown that if the forcings are excited equally and define a unitary transformation in the space spanned by their range, then the ensemble average statistics are independent of the forcing distribution (Farrell and Ioannou 1993c). In Farrell and Ioannou (1993b), we described a method for obtaining a complete set of orthogonal forcings (FOFs) ordered according to their contribution to the variance (this set is distinct from both the EOFs and the normal modes of the evolution operator). Convergence requires that the minimum scale of the forcing be adequate to resolve the structure of the leading forcing orthogonal functions (FOFs). For $k = 2$ and $l = 2$ a forcing distribution

with a minimum resolved scale of 0.5 km is necessary (Farrell and Ioannou 1993b). For longer waves this minimum vertical scale is larger. For example, the first FOF and EOF for waves with $k = 1$ and $l = 1$ are plotted in Figs. 3a,b, and it is evident from this figure that a minimum resolved scale in the forcings of ~3.5 km is adequate. If we insist—as we will for simplicity—that all resolved scales are forced equally, then we will overestimate the total forcing required to maintain the variance and associated fluxes at the largest scales (by a factor of 2–5). Highly resolved calculations were performed with typically 100 points in the troposphere and with convergence verified by doubling the resolution.

The unique stochastic forcing mechanism has not been identified, but the forcing is thought to arise primarily from two sources: diabatic heating and spectral scattering due to nonlinear processes. A rate of wave scale energy injection $E_{in} = 0.7$ W m^{-2} is typically found in energy budget analyses of the Lorenz cycle (Peixoto and Oort 1992), and in addition O(20 W m^{-2}) (Peixoto and Oort 1992) of diabatic heating are available; however, most of this heating contributes primarily to the maintenance of the large-scale static stability of the midlatitude troposphere against destabilization by radiative cooling. The coupling of diabatic heating on the cloud-scale to synoptic-scale geostrophically balanced motions depends on the spatial and temporal scales of the heating (Blumen 1972), and the efficiency of this coupling is uncertain. If we arbitrarily assume an efficiency of 1%, we would then obtain a forcing rate of O(0.2 W m^{-2}) from this source. Such considerations suggest that wave-scale energy injection rates of 1 W m^{-2} are not unreasonable.

The statistics of baroclinic waves on a subcritical mean state is studied in this work, and our hypothesis is that the midlatitude atmospheric statistics can be understood as the nonnormal response to stochastic forcing of the linearized quasigeostrophic equations with appropriate choice of parameters. The mean atmospheric state is maintained in the subcritical regime by parameterizing the disruption arising from wave–wave interactions so as to ensure stability. This role of nonlinearity in turbulence was referred to as scrambling by Salmon (1980) in his investigation of quasigeostrophic turbulence. The linear potential vorticity damping that parameterizes the scrambling effect may depend on wavenumber and eddy activity, as in the TFM model of stochastic turbulence (Herring and Kraichnan 1972; Leith and Kraichnan 1972; Leith 1971). Nevertheless, in the examples to follow we obtain satisfactory results using a simple potential vorticity damping that does not vary with wavenumber. The likely reason for the success of this simple choice of damping is that the wave energetics is dominated by the linear operator in this strongly sheared flow, while in homogeneous isotropic turbulence the dominance of the nonlinearity means that this parameterization by itself determines the response. It should be noted that this assumed dominance of the linear operator is not expected to be valid for regimes characterized by sufficiently small shear.

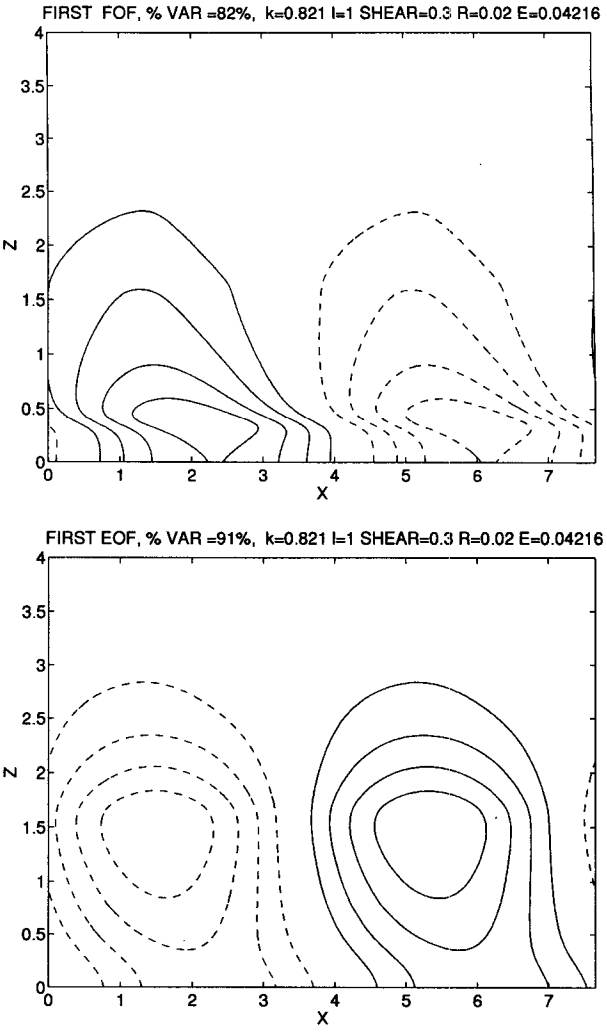

FIG. 3. (a) The first FOF (the forcing distribution that gives rise to most of the variance), which forces 82% of the maintained ensemble average energy. (b) The first EOF of the correlation matrix, which accounts for 91% of the ensemble average energy. The case shown is for waves with $k = 0.821$, which corresponds to global wavenumber 5, $l = 1$, and a mean flow with $s = 0.3$, $R = 0.02$, and $\nu = 20$ m^2 s^{-1}. Contours of stream function ϕ are shown.

The most crucial parameters determining the asymptotic stability of the flow are the imposed potential vorticity damping R and the meridional wavenumber l. For the mean winter jet with a maximum zonal velocity of 35 m s^{-1} and boundary-layer vertical eddy diffusion coefficient $\nu = 20$ m^2 s^{-1}, baroclinic waves with meridional wavenumber $l = 2$ are within the asymptotically stable regime for linear damping timescales R^{-1} of order 10 days. Stabilization of waves with meridional wavenumber $l = 1$ requires damping timescales R^{-1} of at most 6 days. It should be noted that $l \approx 1$ is

the meridional wavenumber of the most exponentially unstable mode of the midlatitude atmospheric jet (Ioannou and Lindzen 1986; Lin and Pierrehumbert 1988). With linear damping of order 6 days the jet is subcritical but close to the stability boundary at this meridional scale.

Robust transient growth due to nonnormality of the dynamical operator rather than accumulation of energy due to modal resonance is found to dominate the statistics at synoptic scales even for the $l = 1$ perturbations, which are located close to the stability boundary. As an example of the transient growth mechanism, the maximal energy growth possible at different times is shown in Fig. 4. Perturbations with global zonal wavenumber $m = 5$ and 18 (dimensionless $k = 0.821$ and 3, respectively) and a linear damping with e-folding time of approximately 6 days were chosen. The maximal energy growth at time t is given by $\|e^{\mathcal{A}t}\|_2^2$, where the subscript 2 denotes the Euclidean norm. Note that Fig. 4 does not trace the energy of a specific perturbation as a function of time but rather the maximum growth of the optimal perturbation for the indicated time. For wavenumber 5 the global optimal growth (the maximal energy growth over all optimizing times) requires 15 days, while for wavenumber 18 this optimal occurs at 9 days.

That the midlatitude jet is maintained in proximity to the stability boundary can be inferred from the sharp peak at zonal wavenumbers $m \approx 5$ in the observed wavenumber–period spectra of the midlatitude transient geopotential variance as seen in Fig. 5 (cf. Hayashi and Golder 1977; Fraedrich and Böttger 1978; Schafer 1979; Hansen et al. 1989). Calculations of the variance as a function of wavenumber and period were performed for $l = 1$ with linear damping sufficient so that the atmospheric state is stable but close to the stability boundary. The frequency response (cf. Farrell and Ioannou 1993b) is given by

$$F(\omega) = \mathrm{trace}(\mathcal{R}^\dagger(\omega)\mathcal{R}(\omega)) = \|\mathcal{R}(\omega)\|_F^2, \quad (3.1)$$

where the subscript F denotes the Frobenius norm and the resolvent $\mathcal{R}(\omega)$ is given by

$$\mathcal{R}(\omega) = (i\omega I - \mathcal{A})^{-1}, \quad (3.2)$$

with I the identity and ω the frequency. The resulting power spectrum is shown in Fig. 6. The close resemblance of this spectrum to the observed spectrum in Fig. 5 suggests that an equivalent potential vorticity damping maintains the flow near neutrality. For higher dissipations and/or for short meridional wavelengths for which the flow is far from the stability boundary, the spectra do not show the observed sharp peak and dispersive structure; instead, the stochastic response exhibits a broad maximum at synoptic time and space scales.

Both the magnitude and dispersive structure of the power spectrum arise primarily from the nonnormality of the evolution operator $\mathcal{A}$. In order to isolate the crucial role of nonnormality from that of the more familiar modal resonance mechanism arising from proximity of the poles to the real axis, which occurs in normal systems, we calculate the power spectrum (3.1) for the equivalent normal operator $\mathcal{A}_{\text{normal}}$, which is defined as the diagonal operator with the same eigenvalues as $\mathcal{A}$ and therefore the same modal resonance behavior. For $\mathcal{A}_{\text{normal}}$, the peaks in the power spectrum occur at fre-

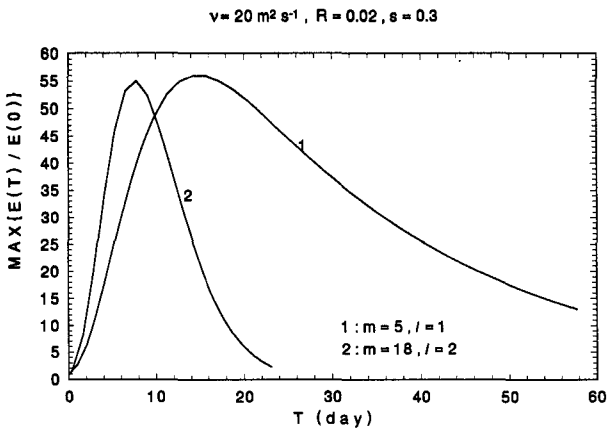

FIG. 4. Maximal energy growth that can be achieved as a function of time in days. Curve 1 is for global zonal wavenumber $m = 5$ (nondimensional $k = 0.821$) and nondimensional meridional $l = 1$. Curve 2 is for global zonal wavenumber $m = 18$ (nondimensional $k = 3$) and nondimensional meridional $l = 2$. The linear damping is $R = 0.02$ corresponding to an e-folding time of 6 days; the vertical diffusion coefficient is $\nu = 20\ \mathrm{m^2\ s^{-1}}$. The baroclinic basic state has shear $s = 0.3$, corresponding to a maximum jet speed at the tropopause of 35 m $\mathrm{s^{-1}}$.

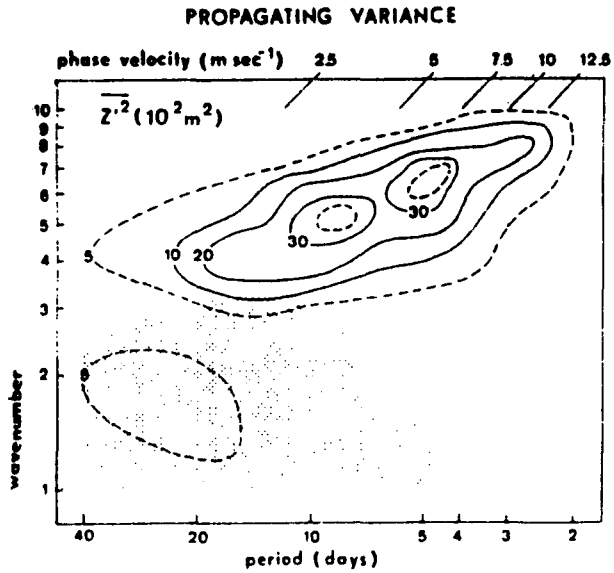

FIG. 5. Power spectrum of geopotential at 500 mb and 50°N averaged over the winter seasons between 1972 and 1973 (from Fraedrich and Böttger 1978).

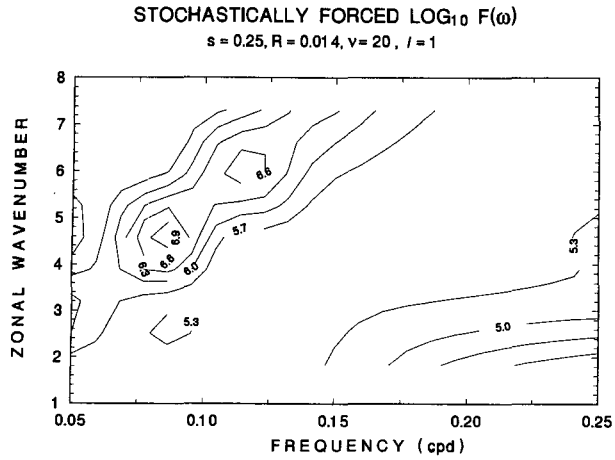

FIG. 6. The power spectrum as a function of frequency (in cycles per day) and global zonal wavenumber. This spectrum is obtained from stochastic forcing of a baroclinic jet with nondimensional shear parameter $s = 0.25$, linear damping of $R = 0.014$ (corresponding to an e-folding time of 8 days), and vertical diffusion coefficient $\nu = 20$ m^2 s^{-1}. The nondimensional meridional wavenumber is $l = 1$.

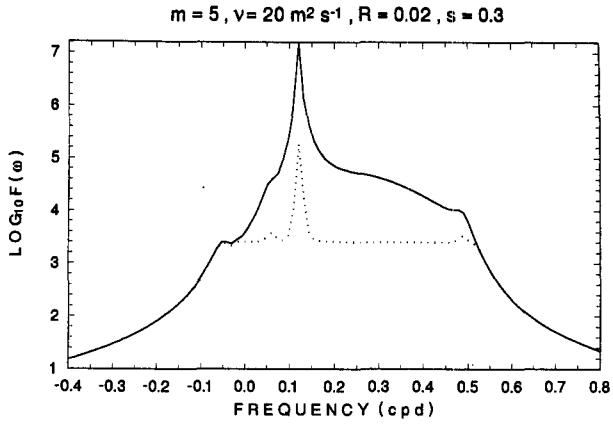

FIG. 8. The power spectrum as a function of frequency (in cycles per day) for global zonal wavenumber 5. This spectrum is obtained from stochastic forcing of a baroclinic jet with nondimensional shear parameter $s = 0.3$, linear damping of $R = 0.02$ (corresponding to an e-folding time of 6 days), and vertical diffusion coefficient $\nu = 20$ m^2 s^{-1}. The nondimensional meridional wavenumber is $l = 1$. The dotted line corresponds to the maintained variance obtained from the equivalent normal evolution operator. Note the sharp peak for a period of approximately 10 days.

quencies close to the poles of the resolvent, and the peak magnitude is inversely proportional to the square of the distance to the poles, as in a normal dynamical system. The power spectrum of $\mathscr{A}_{\text{normal}}$ is shown in Fig. 7. Note that although the equivalent normal response shows a peak for wavenumber 5 with an approximate period of 10 days, the magnitude is underestimated by nearly two orders of magnitude, and furthermore, the power spectrum does not exhibit the observed dispersive properties so well captured by the nonnormality, as shown in Fig. 6.

The prominence of wavenumber 5 in the transient spectrum during the Southern Hemisphere summer season is confirmed by the observations of Salby (1982), Schoeberl and Krueger (1983), and Randel and Stanford (1985). The variation with frequency of the power spectrum maintained by stochastic forcing for this wavenumber as shown in Fig. 8 reveals that the stochastic model accurately reproduces the observations for parameters for which the model atmosphere is near to the stability boundary. Note again the importance of the nonnormality in the response. The stochastically

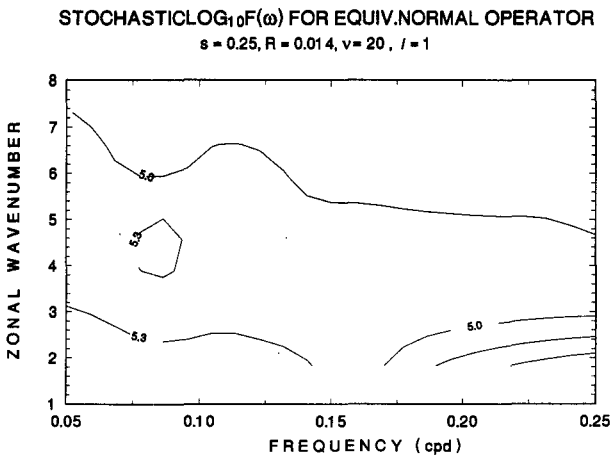

FIG. 7. As in Fig. 2 but for the equivalent normal evolution operator.

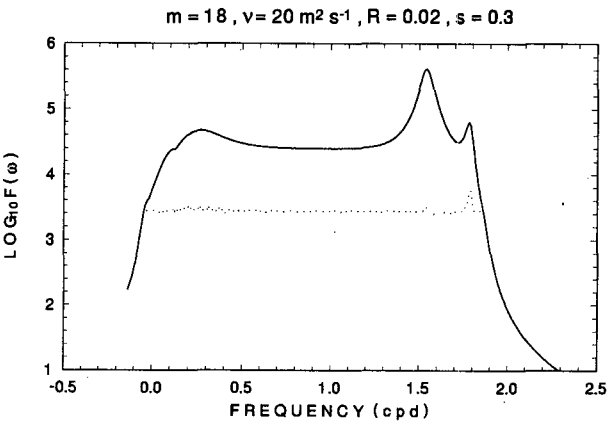

FIG. 9. The power spectrum as a function of frequency (in cycles per day) for global zonal wavenumber 18. This spectrum is obtained from stochastic forcing of a baroclinic jet with nondimensional shear parameter $s = 0.3$, linear damping of $R = 0.02$ (corresponding to an e-folding time of 6 days), and vertical diffusion coefficient $\nu = 20$ m^2 s^{-1}. The nondimensional meridional wavenumber is $l = 1$. The dotted line corresponds to the maintained variance obtained from the equivalent normal evolution operator. The higher-frequency peak corresponds to the upper-level variance concentrated near the tropopause.

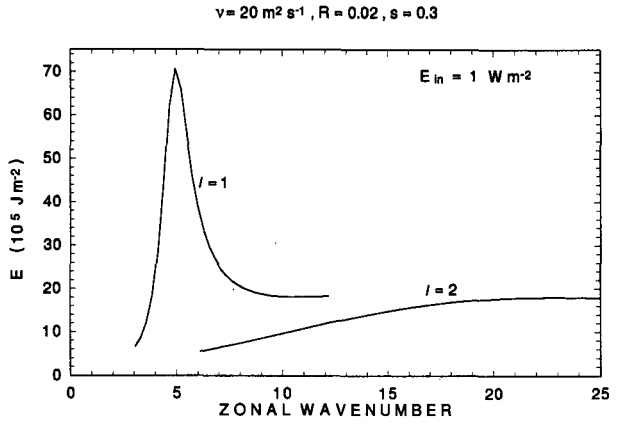

FIG. 10. Ensemble average energy as a function of global wavenumber m, with meridional wavenumber $l = 1$ and $l = 2$, shear $s = 0.3$, and energy input rate $E_{in} = 1$ W m^{-2}. The linear damping parameter is $R = 0.02$ and the coefficient of vertical diffusion is $\nu = 20$ m^2 s^{-1}.

maintained spectrum for $m = 18$ with parameters for which the flow is far from the stability boundary is shown in Fig. 9. Note the enhanced variance at high frequencies associated with an upper-level variance peak as is observed. The equivalent normal response does not show this upper-level peak, which results from the nonnormality of the operator. Incidentally, a conceptually related nonnormal interpretation of the upper-level variance has previously been discussed by Rivest and Farrell (1992) in connection with a theory for the origin of short waves.

The observed average total transient energy in the midlatitude atmosphere is $\langle E \rangle \approx 25 \times 10^5$ J m^{-2} associated with a heat flux over a latitude circle of $\langle H \rangle \approx 1$–$4$ ($\times 10^{15}$ W) (Peixoto and Oort 1992), with marked seasonal variations. It is of interest to determine the magnitude of E_{in} needed to obtain observed atmospheric values of ensemble average transient energy and heat flux. Given that ensemble average quantities depend linearly on the magnitude of the stochastic forcing, we can calculate ensemble averages without loss of generality based on $E_{in} = 1$ W m^{-2}. The required E_{in} that matches observed atmospheric values can then be obtained by scaling the resulting magnitudes.

The variation of the ensemble average energy and heat flux as a function of the global zonal wavenumber m (at 45° this wavenumber is related to the nondimensional wavenumber by $k = 0.821m/5$) and for $l = 1$ and $l = 2$ [corresponding to meridional confinement in a channel of halfwidth (in dimensional variables) $\tilde{y}_c \approx \pi L/2l \approx 1200$ and 600 km, respectively] is shown in Figs. 10 and 11. These calculations correspond to mean winter conditions for which the vertical shear has been taken to be $s = 0.3$, which for latitude $\phi = 45°$ corresponds through the discrete version of the thermal wind relation:

$$\frac{\Delta T_g}{\Delta y} = \frac{f_0 T_g}{g} \frac{U_m}{H_t}, \tag{3.3}$$

to $\Delta T_g \approx 30$ K, where $\Delta T_g(\phi) \equiv T_g(\phi - 15°) - T_g(\phi + 15°)$ [in (3.3) T_g is the ground temperature, g is the gravitational acceleration, Δy is the distance over 30° of latitude, U_m is the dimensional velocity at the jet maximum, and $H_t = 1.5H$ is the tropopause height]. Such a meridional temperature gradient is characteristic of Northern Hemispheric winter conditions at $\phi = 45°$. For the $l = 1$ simulation both the maintained energy and the associated heat flux show a prominent maximum at wavenumber 5. This is characteristic of parameters for which the flow is near the stability boundary. A. Solomon performed analysis of the January average heat flux in both hemispheres as a function of zonal wavenumber using the ECWMF dataset spanning the period from 1979 to 1988. Her analysis, shown in Fig. 12, reveals the sensible heat flux peak at zonal wavenumber 5 in both hemispheres. The prominence of wavenumber 5 is affected by linear damping. For linear damping with R^{-1} of 5 days, the peak is reduced considerably and the variance and heat flux resemble results from the $l = 2$ simulation, which are characteristic of flows far from the stability boundary for which the ensemble average energy and heat flux exhibit a broad maximum at high zonal wavenumber.

The ensemble average energetics for the winter months is shown in Fig. 13. Note that the ensemble average perturbation energy balance is between the transfer of energy from the mean and dissipation (which for these parameters is shared equally between dissipation due to Ekman spindown and linear damping) rather than between forcing and dissipation. This is a characteristic property of stochastic excitation of nonnormal dynamical systems, which maintain ensemble average energies and energy transfers far in excess

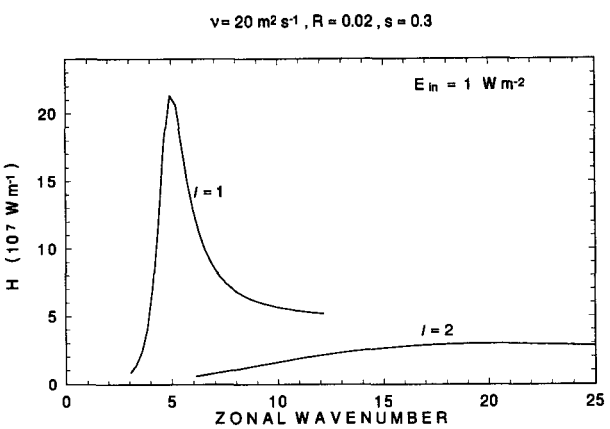

FIG. 11. Ensemble average heat flux as a function of zonal global wavenumber m, with meridional wavenumber $l = 1$ and $l = 2$; shear $s = 0.3$, and energy input rate $E_{in} = 1$ W m^{-2}. The linear damping parameter is $R = 0.02$, and the coefficient of vertical diffusion is $\nu = 20$ m^2 s^{-1}.

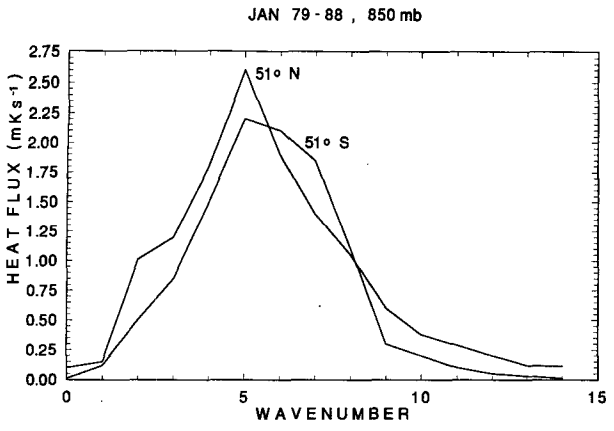

FIG. 12. Average transient heat flux at 850 mb as a function of global zonal wavenumber during January for the years 1979 to 1988 at 51° in the Northern and Southern Hemispheres at 850 mb. The analysis of the ECMWF dataset was performed by Amy Solomon.

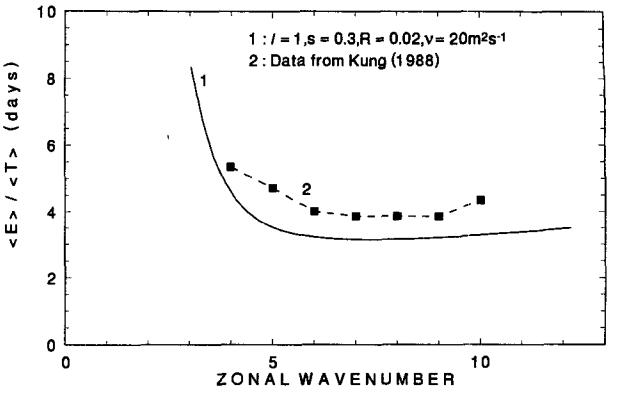

FIG. 14. The variation of dissipation time scale t_d as a function of wavenumber. The continuous curve is for $l = 1$, $R = 0.02$, and $\nu = 20$ m^2 s^{-1}. The dot curve is compiled from the values given in Kung (1988).

of those supported by similarly damped forced-dissipative normal systems. Consequently, the dissipation timescale

$$t_d = \frac{\langle E \rangle}{D_{\text{atm}} + D_{\text{Ekman}}} \tag{3.4}$$

can be approximated by

$$t_d \approx \frac{\langle E \rangle}{T}, \tag{3.5}$$

a quantity that can be easily estimated from observations. Budget analyses of the Lorenz cycle for the midlatitude winter season give $t_d = 6$–10 days (Peixoto and Oort 1992; Wiin-Nielsen and Chen 1993). In this estimate, however, the contribution of the stationary and/or standing waves is a confounding factor. It is best for the purpose of comparison with our calculations to calculate t_d based on a spectral analysis of the energetics. Such an analysis by Kung (1988) yields an estimate of $t_d \approx 4.5$. The dynamical timescale obtained from our stochastic model, which is shown as a function of global wavenumber in Fig. 14, reveals encouraging agreement with the timescales derived from the data of Kung (1988) [note that we did not plot the timescales for $m \leq 3$ because Kung (1988) does not use the method developed by Hayashi (1979) to distinguish between standing and traveling waves].

The vertical distribution of the ensemble average energy revealing the observed tropospheric maximum is shown in Fig. 15. The vertical distribution of the heat flux for conditions for which the flow is close to the stability boundary is shown in Fig. 16. Note that the

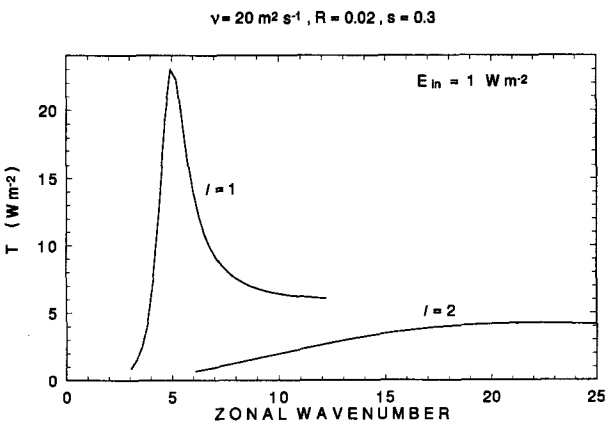

FIG. 13. Ensemble average energy transfer rate T between the mean and eddies, as a function of the zonal wavenumber m, with meridional wavenumber $l = 1$ and $l = 2$; shear $s = 0.3$, and energy input rate $E_{in} = 1$ W m^{-2}. The linear damping parameter is $R = 0.02$ and the coefficient of vertical diffusion is $\nu = 20$ m^2 s^{-1}.

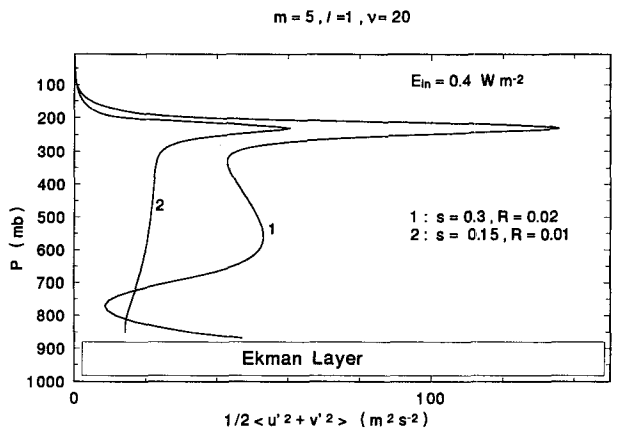

FIG. 15. Variation of the ensemble average kinetic energy per unit mass with height for zonal wavenumber 5 and meridional wavenumber $l = 1$ component. The basic state is the same as in Fig. 1. For the winter months $s = 0.3$, $R = 0.02$, for the summer months $s = 0.15$, $R = 0.01$, and $E_{in} = 0.4$ W m^{-2}.

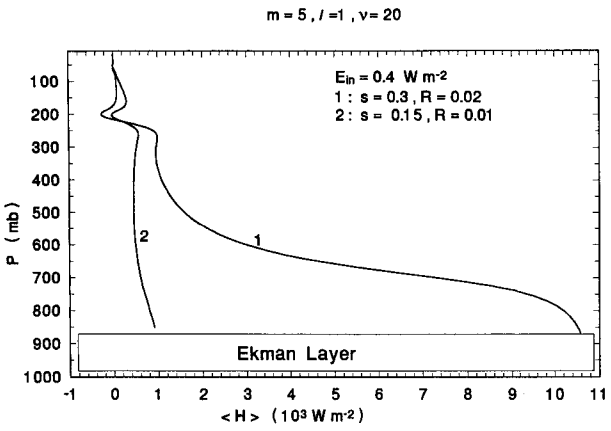

FIG. 16. Distribution of the heat flux with height for zonal wavenumber 5 and meridional wavenumber $l = 1$. The basic state is the same as in Fig. 1. For the winter months $s = 0.3$, $R = 0.02$, for the summer months $s = 0.15$, $R = 0.01$, and $E_{in} = 0.4$ W m^{-2}.

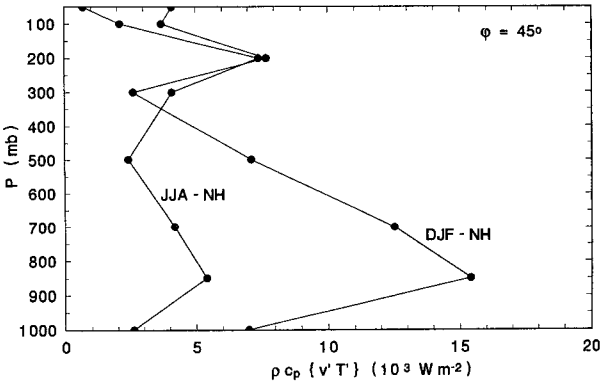

FIG. 17. Variation of the zonally and seasonally averaged transient heat flux at latitude 45°N. The graph is based on the values given by Oort and Peixoto (1983). DJF denotes the winter months, JJA denotes the summer months.

negative heat flux in the stratosphere is associated with downgradient baroclinic transfers. The realism of the distribution can be assessed by comparison to observed fluxes plotted in Fig. 17 (see also Trenberth 1992). Atmospheric values of ensemble average energy and heat flux are produced for $E_{in} \approx 0.5$ W m^{-2}, linear damping of $(6\ \mathrm{d})^{-1}$, and Ekman spindown based on an eddy viscosity $\nu = 20$ m^2 s^{-1}. An exact value of the random forcing is not determined because a change in the dissipation parameters can modulate the resulting ensemble averages over a range of values. What is important to note is that this theory can produce the observed level of ensemble average statistics with reasonable values of forcing.

Theoretical studies (Green 1970; Stone 1972; Held 1978) suggest that the heat flux is strongly dependent on the mean meridional temperature gradient. Stone and Miller (1980) found, based on the heat flux data of Oort and Vonder Haar (1976), that midlatitude atmospheric sensible heat fluxes (stationary and transient) are correlated at the 97% level with variation of the mean temperature gradient at the ground. A similar if somewhat lower correlation is also exhibited by the transient eddy fluxes alone. We have plotted in Fig. 18 monthly averages of the atmospheric heat transports in both hemispheres as a function of the corresponding average temperature gradients ΔT_g taken from Carissimo et al. (1985) and Oort and Peixoto (1983). For comparison, the heat flux that results from stochastic excitation of the corresponding atmospheric flow for conditions far from the stability boundary and linear potential damping and stochastic forcing independent of the eddy activity is also shown in Fig. 18. We argued previously that the evidence of the predominance of wavenumber 5 suggests that the atmosphere operates close to the stability boundary. If R is kept constant at the value appropriate for winter conditions, however, then the heat transport is a highly nonlinear function of the meridional temperature gradient as summer values of ΔT_g are approached, in disparity with the observations, which show an approximately linear relation between the heat flux and the meridional temperature gradient over the seasonal cycle. If we assume that the atmosphere is maintained near neutral stability over the seasonal cycle by the linear potential vorticity damping R, which parameterizes the scrambling effect of the wave–wave interactions, the observed nearly linear flux/gradient relationship requires also changing the stochastic forcing, which parameterizes the nonlinear scattering. Enhanced eddy activity at higher meridional temperature gradient is expected to increase both the scrambling effect and the stochastic forcing. In light of these considerations, we could determine an operating regime of the atmosphere for the winter and summer

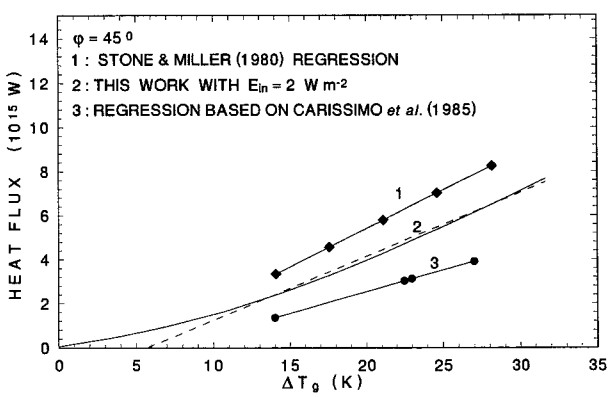

FIG. 18. Variation of the total ensemble average heat flux at 45°N as a function of ΔT_g. Curve 2 is the result of stochastic forcing of the model atmospheric jet for $k = 2$, $l = 2$, $R = 0.01$, $\nu = 20$ m^2 s^{-1}, and $E_{in} = 2$ W m^{-2}. The dash curve is a linear fit. Curve 1 has been compiled by Stone and Miller (1980) based on observations of seasonally averaged heat flux. Curve 3 is based on the seasonally averaged observations of Carissimo et al. (1985).

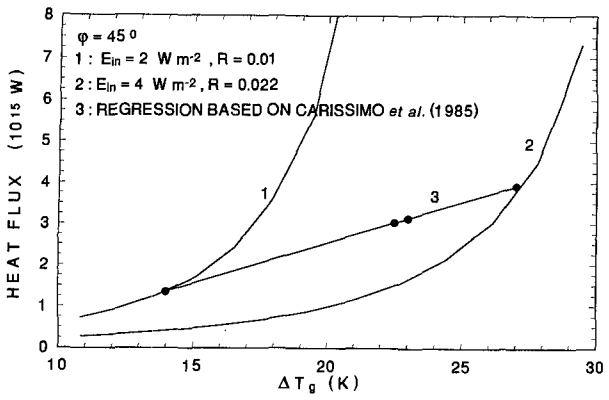

FIG. 19. Variation of the total ensemble average heat flux at 45°N as a function of ΔT_g. Curve 1 is the result of stochastic forcing of the model atmospheric jet for wavenumber 5 ($k = 0.821$), $l = 1$, $R = 0.01$, $\nu = 20$ m^2 s^{-1}, and $E_{in} = 2$ W m^{-2}. Curve 2 is the result of stochastic forcing of the model atmospheric jet for zonal wavenumber 5 ($k = 0.821$), meridional wavenumber $l = 1$, $R = 0.02$, $\nu = 20$ m^2 s^{-1}, and $E_{in} = 4$ W m^{-2}. Curve 3 is based on the seasonally averaged observations of Carissimo et al. (1985).

months by matching the heat flux obtained from Carissimo et al. (1985) while requiring that the atmosphere be always close to the stability boundary. The results of such a calculation are shown in Fig. 19. For the winter months, a damping rate of $R^{-1} \approx 5.5$ days and $E_{in} = 4$ W m^{-2} is required, while for the summer months the observations can be matched with a damping rate of $R^{-1} \approx 11$ days and $E_{in} = 2$ W m^{-2}. Intermediate values shown in Fig. 19 could be obtained similarly by modification of the stochastic driving and the damping rate so as to maintain near neutrality. While these considerations do not lead directly to a simple parameterization for transient eddy heat flux for use in climate models, understanding of the role played by nonnormal dynamics, if confirmed, should permit useful extrapolations of the observed flux/gradient relation to be made.

4. Conclusions

In this work, the calculus developed in Farrell and Ioannou (1993b) to obtain the statistical response of stochastically forced nonnormal dynamical systems has been applied to a model of the baroclinic midlatitude atmosphere in order to find the ensemble average energy spectrum and sensible heat flux arising from transient waves. The theory developed in this work takes advantage of the fact that the dominant dynamics of strongly sheared flow arises from the linear component associated with advection. This linear dominance, reflected in the nonnormality of the dynamical operator, allows the crucial but subdominant nonlinear effects to be parameterized. The parameterized effects of nonlinearity are scattering of disturbances among scales, which is modeled as stochastic forcing, and scrambling or disruption by wave–wave interaction, which is modeled by enforcing an appropriate decorrelation timescale through the choice of dissipation parameter R. This linear potential vorticity damping R maintains the flow subcritical as is required by the finiteness of the observed variance. With appropriate choices of forcing and dissipation, the resulting statistical steady state produces magnitudes and structures of ensemble average energy and heat flux in agreement with midlatitude atmospheric observations and, in addition, produces the observed balance between baroclinic conversions and damping. When viewed from the perspective of nonnormal stochastic dynamics, the prominence of traveling wavenumber 5 in the midlatitude climatology reveals that the atmosphere is operating close to the stability boundary. Given the slight subcriticality of the flow, the observed relation between heat flux and meridional temperature gradient implies a variation of the effective damping rate and magnitude of stochastic forcing over the seasonal cycle.

Over the spectral interval in which the energetically dominant traveling baroclinic waves occur (global wavenumbers $4 < k < 10$) we find that nonnormal stochastic dynamics accounts for both the amplitude and dispersive properties of the waves. A subject of considerable historical interest in atmospheric dynamics concerns the amplitude spectrum of waves $10 < k < 20$, which account for relatively little total wave energy but which appear to follow an approximate k^{-3} power dependence (Kao and Wendell 1970). Evidence from energetic analyses (Kung 1988) suggests that these short waves are not associated with the nonnormal balance between energy gained from the zonal flow and dissipation but rather that these waves exhibit normal system energetics associated with a balance between forcing and dissipation. From our stochastic point of view, this implies that the effective damping at these scales is large enough so that the linear operator is dominated by its diagonal component proportional to R and is therefore effectively normal. One interpretation of the dynamics of these short waves is that they obtain energy from advective frontogenesis and dissipate this energy locally in spectral space as described by Andrews and Hoskins (1978).

The large—indeed, divergent—amplitude and heat flux produced in a stochastically forced but subcritical system as neutrality is approached suggests reinterpretation of theories involving adjustment to neutrality of unstable flows. Examples of such adjustment mechanisms are found in the baroclinic adjustment theories of Stone (1978), Lindzen and Farrell (1980), and Lindzen (1993). According to theories of this kind, the fluxes, arising from modal instability, relax the unstable gradient toward a state of marginal stability. However, as we have seen, the response of such a system to noise sources is divergent near the critical operating point required by the adjustment theories. We therefore suggest that these theories be reinterpreted in the following

way: under inevitable stochastic excitation the fluxes rise as thermal forcing moves the system toward a stability boundary so that the divergent fluxes so produced prevent the system from ever crossing the stability boundary so that instability never occurs.

Together with recent work on the variance arising from stochastic forcing (Farrell and Ioannou 1993a,b), this work provides a theoretical framework for interpreting the dynamics of the midlatitude atmosphere. In contrast to instability theory in which the initial perturbation is unimportant if nonzero, this theoretical point of view stresses the importance of perturbations that provide the required stochastic forcing. In addition, requirements for resolution in modeling the atmosphere are implied: it is necessary to resolve the structures that contribute substantially to producing the correlation matrix (FOFs) as well as to resolve the EOFs of the correlation matrix itself. These forcing structures can be found as solutions to a Lyapunov equation (Farrell and Ioannou 1993b) and resolving these structures requires resolving up to 30 wavenumbers in the troposphere at global wavenumber 15, although at the scales of maximum transient energy and flux (global wavenumbers 4–6), as few as four vertical waves appear to be adequate.

Turning to the question of the sensitivity of the heat flux to variation of the climate system, we note that the primary sensitivities are to the strength of the driving and the dissipation, with factors such as the static stability, the tropopause height, or the latitude playing a relatively minor role. This result suggests that careful study of the physical mechanisms providing perturbations to the system and determining the decorrelation timescale of the perturbations is necessary to gain a deeper understanding of the midlatitude climate.

Acknowledgments. We thank Peter Stone especially for drawing our attention to the wavenumber 5 observations, Amy Solomon for allowing us to use her heat flux analysis, Isaac Held and an anonymous reviewer for meticulous reviewing, and Richard Lindzen for numerous discussions. Petros J. Ioannou was supported by NSF ATM-9216189. B. F. Farrell was supported by DOE through the Northeast Regional Center of NIGEC by NSF ATM-9216813. Financial support does not constitute an endorsement by DOE of the views expressed in this article.

REFERENCES

Andrews, D. G., and B. J. Hoskins, 1978: Energy spectra predicted by semigeostrophic theories of frontogenesis. *J. Atmos. Sci.*, **35**, 509–512.

Blumen, W., 1972: Geostrophic adjustment. *Rev. Geophys. Space Phys.*, **10**, 485–528.

Carissimo, B. C., A. H. Oort, and T. H. Vonder Haar, 1985: Estimating the meridional energy transport in the atmosphere and the ocean. *J. Phys. Oceanogr.*, **15**, 82–91.

Charney, J. G., 1947: The dynamics of long waves in a baroclinic westerly current. *J. Meteor.*, **4**, 135–162.

——, and M. Stern, 1962: On the stability of internal baroclinic jets in a rotating atmosphere. *J. Atmos. Sci.*, **19**, 159–172.

Eady, E. T., 1949: Long waves and cyclone waves. *Tellus*, **1**, 33–52.

Farrell, B. F., 1982: The initial growth of disturbances in a baroclinic flow. *J. Atmos. Sci.*, **39**, 1663–1686.

——, 1984: Modal and nonmodal baroclinic waves. *J. Atmos. Sci.*, **41**, 668–673.

——, 1985: Transient growth of damped baroclinic waves. *J. Atmos. Sci.*, **42**, 2718–2727.

——, 1989: Optimal excitation of baroclinic waves. *J. Atmos. Sci.*, **46**, 1193–1206.

——, and P. J. Ioannou, 1993a: Stochastic forcing of perturbation variance in unbounded shear and deformation flows. *J. Atmos. Sci.*, **50**, 200–211.

——, and ——, 1993b: Stochastic dynamics of baroclinic waves. *J. Atmos. Sci.*, **50**, 4044–4057.

——, and ——, 1993c: Stochastic forcing of the linearized Navier–Stokes equations. *Phys. Fluids A*, **5**, 2600–2609.

Ferrel, W., 1881: Meteorological researches for the use of the coast pilot. Part II: On cyclones, tornadoes and watersprouts. *U.S. Coast Geodetic Survey*, App. 10.

Fraedrich, K., and H. Böttger, 1978: A wavenumber–frequency analysis of the 500 mb geopotential at 50°N. *J. Atmos. Sci.*, **35**, 745–750.

Gall, R., 1976: Structural changes of growing baroclinic waves. *J. Atmos. Sci.*, **33**, 349–373.

——, R. Blakeslee, and R. C. J. Somerville, 1979: Baroclinic instability and the selection of the zonal scale of the transient eddies of middle latitudes. *J. Atmos. Sci.*, **36**, 767–784.

Green, J. S. A., 1970: Transfer properties of the large-scale eddies and the general circulation of the atmosphere. *Quart. J. Roy. Meteor. Soc.*, **96**, 157–185.

Hansen, A. R., A. Sutera, and D. E. Venne, 1989: An examination of midlatitude power spectra: Evidence for standing variance and the signature of El Niño. *Tellus*, **41A**, 371–384.

Hayashi, Y., 1979: A generalized method for resolving transient disturbances into standing and traveling waves by space–time spectral analysis. *J. Atmos. Sci.*, **36**, 1017–1029.

——, and D. G. Golder, 1977: Space–time spectral analysis of midlatitude disturbances appearing in a GFDL general circulation model. *J. Atmos. Sci.*, **34**, 237–262.

Held, I. M., 1978: The vertical scale of an unstable baroclinic wave and its importance for eddy heat flux parameterizations. *J. Atmos. Sci.*, **35**, 572–576.

Herring, J. R., and R. H. Kraichnan, 1972: Comparison of some approximations for isotropic turbulence. *Statistical Models and Turbulence*, M. Rosenblatt and C. V. Atta, Eds., Springer-Verlag, 148–173.

Ioannou, P. J., and R. S. Lindzen, 1986: Baroclinic instability in the presence of barotropic jets. *J. Atmos. Sci.*, **43**, 2999–3014.

Joseph, D. D., 1976: *Stability of Fluid Motions I.* Springer-Verlag, 282 pp.

Kao, S.-K., and L. Wendell, 1970: The kinetic energy of the large scale atmospheric motion in wavenumber frequency space. *J. Atmos. Sci.*, **27**, 376–387.

Kung, E. C., 1988: Spectral energetics of the general circulation and time spectra of transient waves during the FGGE year. *J. Climate*, **1**, 5–19.

Leith, C. E., 1971: Atmospheric predictability and two-dimensional turbulence. *J. Atmos. Sci.*, **28**, 145–161.

——, 1973: The standard error of time-average estimates of climatic means. *J. Appl. Meteor.*, **12**, 1066–1069.

——, and R. H. Kraichnan, 1972: Predictability of turbulent flows. *J. Atmos. Sci.*, **29**, 1041–1058.

Lin, S.-J., and R. T. Pierrehumbert, 1988: Does Ekman friction suppress baroclinic instability? *J. Atmos. Sci.*, **45**, 2920–2933.

——, and R. T. Pierrehumbert, 1993: Is the midlatitude zonal flow absolutely unstable? *J. Atmos. Sci.*, **50**, 505–517.

Lindzen, R. S., 1993: Baroclinic neutrality and the tropopause. *J. Atmos. Sci.*, **50**, 1148–1151.

——, and B. F. Farrell, 1980: The role of polar regions in global climate and a new parameterization of global heat transport. *Mon. Wea. Rev.*, **108,** 2064–2079.

North, G. R., 1975: Theory of energy-balance models. *J. Atmos. Sci.*, **32,** 2033–2043.

Oort, A. H., 1971: The observed annual cycle in the meridional transport of atmospheric energy. *J. Atmos. Sci.*, **28,** 325–339.

——, and T. H. Vonder Haar, 1976: On the observed annual cycle in the ocean–atmosphere heat balance over the Northern Hemisphere. *J. Phys. Oceanogr.*, **6,** 781–800.

——, and J. P. Peixoto, 1983: Global angular momentum and energy balance requirements from observations. *Advances in Geophysics,* Vol. 25, Academic Press, 355–489.

Peixoto, J. P., and A. H. Oort, 1992: *Physics of Climate.* Amer. Inst. Phys., 520 pp.

Randel, W. J., and J. L. Stanford, 1985: An observational study of medium-scale wave dynamics in the Southern Hemisphere summer. Part I: Wave structure and energetics. *J. Atmos. Sci.*, **42,** 1172–1188.

Rivest, C., and B. F. Farrell, 1992: Upper-tropospheric synoptic scale waves. Part II: Maintenance and excitation of quasi-modes. *J. Atmos. Sci.*, **49,** 2120–2138.

Salby, M. L., 1982: A ubiquitous wavenumber-5 anomaly in the Southern Hemisphere during FGGE. *Mon. Wea. Rev.*, **110,** 1712–1720.

Salmon, R. S., 1980: Baroclinic instability and geostrophic turbulence. *Geophys. Astrophys. Fluid Dyn.*, **15,** 167–211.

Schafer, J., 1979: A space–time analysis of tropospheric planetary waves in the Northern Hemisphere geopotential heights. *J. Atmos. Sci.*, **36,** 1117–1125.

Schoeberl, M. R., and A. J. Krueger, 1983: Medium scale disturbances in total ozone during Southern Hemisphere summer. *Bull. Amer. Meteor. Soc.*, **64,** 1358–1365.

Sellers, W. D., 1969: A climate model based on the energy balance of the earth–atmosphere system. *J. Appl. Meteor.*, **8,** 392–400.

Solberg, H., 1928: Integrationen des atmosphärischen Storüngsgleichungen. *Geof. Publ.*, **5,** No. 9, 120 pp.

Stone, P. H., 1972: A simplified radiative–dynamical model for the static stability of rotating atmospheres. *J. Atmos. Sci.*, **29,** 405–418.

——, 1978: Baroclinic adjustment. *J. Atmos. Sci.*, **35,** 561–571.

——, and D. A. Miller, 1980: Empirical relations between seasonal changes in meridional temperature gradients and meridional fluxes of heat. *J. Atmos. Sci.*, **37,** 1708–1720.

Trenberth, K. E., 1992: *Global Analyses from ECMWF and Atlas of 1000 to 10 mb Circulation Statistics,* NCAR/TN-373, 191 pp.

Winn-Nielsen, A., and T.-C. Chen, 1993: *Fundamentals of Atmospheric Energetics.* Oxford University Press, 376 pp.